Alle ord i engelske overskrifter med stor forbokstsv. Bortsett fra and, on etc.

Wide and small angle x-ray scattering on talc filled polypropylene

Eirik Torbjørn Bakken

March 8, 2013

Abstract

Contents

Start intro litt mer generelt, motivasjon for opp, hvorfor det er interessant etc.

Chapter 1

Introduction

This projects was aimed at examining different samples of polypropylene using wide angle x-ray scattering. The experimental work was done at the X-ray group of the institute of physics at the Norwegian University of Science and Technology (NTNU) during four weeks in the period of June to August 2011 under the supervision of Dag W. Breiby and in close collaboration with phd. student Håvard Granlund. Other persons involved in the project at the instiute of physics were phd. student Jostein Bø Fløystad and phd. studen Morteza Esmaeili. It has in addition been included some results from a small-angle x-ray scattering measurement perfomed by Håvard Grandlund and Dag W. Breiby in November 2012. The samples were provided by SINTEF and was manufactured by injection molding. SINTEF was represented in the project through Per Erik Vullum and Erik Andreassen.

The purpose for this project was first and foremost to start examining the polypropylene samples, and get a better understanding of some of the characteristics like structural orientation of the polymers and visibility of the scattered signal, and how they varied through the sample. By performing a raster scan over the different samples, one could extract different parameters for analysis. This was done so one would have the basis for a further study of the material, where one could go in depth on those factors that seemed to be important and relevant for the microscopic structure. The overall goal for the study on these samples of polypropylene was to see how the polymers is oriented inside the sample, and in what way this is varying compared to where the polymer is injected, and compared to the surface normal. The continued work based on this project has been accepted in a scientific paper, and will be published a short time in the future [1].

By studying this sample of polypropylene, it is hoped to gain more insight into the structure of the material. This material is one of the most important plastics in the world, with an estimated worldwide generated revenue of more than US $145 billion in the year 2019. The average growth the past eight years has been 4.4 % and will likely be surpassed in the coming years [2]. With such an important material, it is clear that a good understanding of all its properties is important to realize its full potential. The fact that it is estimated that the material will still be of big importance in many years from now shows that a study of polypropylene is future-oriented.

Skrives x-ray med stor el liten x?

The ability to make a large number of x-ray measurements of different parts of a sample has been possible due to the recent development in X-ray physics, and the establishing of a state of the art home laboratory at the NTNU. For mapping structural differences at sufficient resolution, one needs a beam with a spot size in the range of $\sim$ µm and also step motors which can move the sample with a resolution in the range of $\sim$ mm. The spot size can be focused using different kind of x-ray focusing techniques and the step motors can for example be made by piezo electric motors. The most important factor for mapping different kinds of gradients through the sample is the high resolution electronic detector, which have a small sampling time and fast readout time, preventing the experiment to be too time consuming. The fact that the computer industry is developing increasingly more powerful personal computers also makes it possible to analyze the large data samples in a reasonable time, without expensive high-performance computers.

This report will first give a short introduction to the material polypropylene with known characteristics and a brief history of development. Then a description of the theory, the experiment and analysis will be given, to let the reader understand what kind of knowledge is needed to comprehend the result. This will be followed by the experiment section which will give a brief description of how the experiment was performed, and which areas of the samples were scanned. The section containing the results, discussion and conclusion will contain a discussion and conclusion over the different kind of orientation and visibility plots for the different samples, and compare them to see the similarities and differences between the different samples.

Siste avsnittet er bra, blrtsett fra siste setning. Litt forvirrende og gjentar seg selv litt.

Chapter 2

The sample analyzed

The sample analyzed for the wide-angle x-ray scattering measurement was an isotactic polypropylene sample provided by SINTEF, and was produced by injection molding. Talc had been added to the polypropylene for producing purposes. For the small angle x-ray scattering experiment performed, nine different samples were used. They have the designation *EDXY*, where the two first letters, *ED*, is just referring to the sample type. The third letter, *X*, is referring to the mold temperature and is either *L* (low temperature), *M* (medium temperature) or *H* (high temperature). The last letter, *Y*, refer to the shear rate of which the sample was made. The shear rate is either *L* (low), *M* (medium) or *H* (high). The values for the low, medium and high temperature and shear rate are given in table 2.1

Table 2.1: The values for low, medium and high temperature and shear rate during the manufacturing of the samples.

	Shear rate	Temperature
Low	25 s^{-1}	20° C
Medium	150 s^{-1}	40° C
High	850 s^{-1}	65° C

When neglecting the solidifying layer at the walls the shear rate is given by

$$\dot{\gamma} = 3\frac{Q}{Ah}. \tag{2.1}$$

Here Q is the volumetric flow rate in m^3/s, A the area of the cross section of the dog-bone neck and h is the smallest dimension of the cross section. The shear rate governs the injection speed of the melt and the pressure applied during solidification [3].

2.1 Polypropylene

Polypropylene is a material consisting of a repeating cell of propene, as described in Figure 2.1.

Bildeteksten burde heller bli forklart i den vanlige teksten, og shortened her.

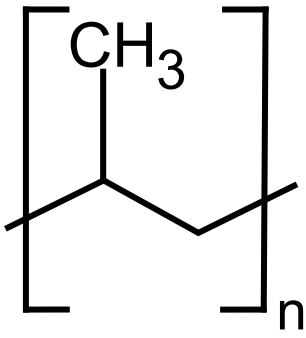

Figure 2.1: The repeating cell of polypropylene. Here n is a number in the range of 10 thousands symbolizing the repeating structure. A carbon atom with two attached hydrogen atoms are placed at each corner.

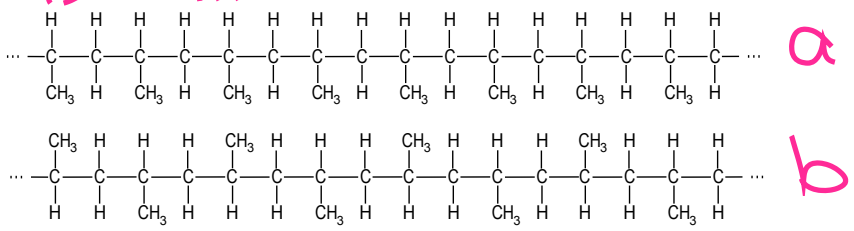

Figure 2.2: Top figure shows isotactic polypropylene, while the bottom one shows syndiotactic polypropylene. Figure adapted from [5].

Fig 2.2: gi de heller navn som a og b enn top/bottom

The material in this study is of the type isotactic polypropylene. This means that the methyl-groups all sit on the "same" side, shown in Figure 2.2, and that the polymer is developing in a straight way, without any sharp bends. Whether the polypropylene is isotactic or not has implications on the polymers ability to form crystals, where lower isotacticity, meaning more defects from a perfect isotactic chain, means smaller crystal size [4].

Hva er a, b, c etc.?

Isotactic polypropylene will crystallize in four different ways; α (monoclinic), β (hexagonal), γ (triclinic) and smectic, where α is usually the far dominant form [6]. The structure of the unit cell in the α form is $a = 0.666$nm, $b = 2.078$nm, $c = 0.6495$nm, $\beta = 99.62°$ and $\alpha = \gamma = 90°$, where the chain is along the c-axis [7]. Which form the polypropylene crystallizes to depends on a number of factors as temperature [8] and shear strength [9]. Decreasing tacticity also has the implication of lower melting temperature and that more of the polypropylene will crystallize in the γ-phase [4].

The polypropylene samples used in this project were injection molded. This is a process where thermoplastics are forced in to a heated barrel where it is melted and mixed, typically by a revolving screw inside the barrel, which also forces the plastic forward from the intake towards the outlet where the mold is attached. The plastic is then injected to the mold cavity which has a colder temperature, cooling and solidifying the plastic almost as soon as the mold is filled. Injection molding is the

Lang setning, del opp?

most used method to produce products of thermoplastics [10].

2.2 Talc

Talc is a mineral with chemical formula $H_2Mg_3(SiO_3)_4$ and crystallizes in a monoclinic unit cell with parameters $a = 5.26$ Å, $b = 9.1$ Å, $c = 18.81$ Å and $\beta = 100°$ [1]. Talc has a number of effects when added to polypropylene. The ability to reinforce polymers [11] is one of the advantages, in addition reducing shrinkage and warpage, and reduce thermal expansion and the cycle time [1]. Better understanding of how the talc behaves inside the talc sample could therefor influence the production procedure, and lead to more customized polypropylene samples.

Hvorfor denne forståelsen
Kan influence prod
kommer ikke helt fram.

Veldig mye"one" her

Chapter 3

Theory

Litt vanskelig å se hva som er motsetningen til classical view.

Litt brå start

3.1 Electromagnetic waves and photons

When dealing with x-rays one can make the two normal distinctions as one will normally do when it comes to different kind of electromagnetic waves. One can either adopt the classical view, and imagining an x-ray beam as a propagating wave in compliance with Maxwells equations, or regarding an x-ray beam as a stream of quantified photons. What kind of description is correct depends on which phenomena one is regarding.

When dealing with x-rays as electromagnetic waves one adopts the formalism by describing the electric part of the wave with complex numbers:

$$\mathbf{E} = \mathbf{E}_0 \mathrm{e}^{i(\mathbf{k}\cdot\mathbf{r}-\omega t)}. \tag{3.1}$$

$\mathbf{k}$ is the wave vector of the electromagnetic beam, ω is the frequency, $\mathbf{r}$ the position vector and t is the time. The complex amplitude vector, $\mathbf{E}_0$, contains both information on the absolute amplitude of the wave, the phase of the wave and the polarization of the wave. Many materials have often refractive index close to unity in the x-ray regime, which means that an electromagnetic waves with these wavelengths considers the material almost similar to vacuum. This means that the polarization is perpendicular to the wave vector k, which follows from Maxwells equations for electromagnetic waves in vacuum. The real electric field is the real part of 3.1. In this representation the electromagnetic wave is considered a plane wave, and this is normally a good approximation when dealing with x-ray scattering, because the wavelength is very small compared to the usual spot size. If one approximates the beam from the x-ray source like a Gaussian beam, the radius of curvature, R is given by:

$$R(z) = z\left(1 + \left(\frac{z_0}{z}\right)^2\right) [12]. \tag{3.2}$$

Henger ikke helt sammen

Here z is the distance from the beam center, and $z_0 = \pi W_0^2/\lambda$[12], is the Rayleigh range, where W_0 is the beam width at the beam center, and λ is the wavelength of the beam. Since the beam width is in the order $\sim 10^{-4}$m, the wavelength is in the order of $\sim 10^{-10}$m and the distance from the beam center is in the order of ~ 1m the radius of curvature will be in the order of $\sim 10^5$m. The area illuminated by

the x-ray beam is in the same order as the beam width, and it is therefore a good approximation to consider the incomming x-ray beam to be a planar wave when it is interacting with a sample.

With this approximations, and considering a wave traveling in the x-direction and polarized in the z-direction in a Cartesian coordinate system, one can write the incoming x-ray beam as:

$$\mathbf{E} = E_0 \sin(k_x x - \omega t)\hat{z}. \tag{3.3}$$

Since it has been mentioned that x-rays can be regarded as particles, a short description will follow regarding the subject. When one is quantifying the electro-magnetic wave, one is visualizing a particle called the photon with quantum energy $E = hf$. E is the energy, h is Planck's constant and f is the frequency of the electromagnetic wave. Viewing x-rays in this manner is important when considering the creation of characteristic x-ray spectra from the x-ray source and inelastic scattering as compton scattering, but will not be handled in more detail here, since it will suffice to know that photons exist to understand the work that has been done.

3.2 Scattering theory

3.2.1 Fundamental theory

The fundamentals of scattering theory lays on the fact that an electron will interact with an incoming electromagnetic beam, or photon, depending on which representation is most fitting. In most x-ray scattering experiments one assume that the scattering is elastic. This means that the scattered wave has the same wavelength as the incoming photon. When considering scattering from a single electron, one imagines that the incoming electromagnetic wave will act with a force on the electron, and hence start to accelerate it. This will again cause the electron to radiate according to:

$$\frac{dP}{d\Omega} = \frac{e^2}{16\pi^2\epsilon} \frac{|\hat{\mathbf{r}} \times (\mathbf{u} \times \mathbf{a})|^2}{(\hat{\mathbf{r}} \cdot \mathbf{u})^5} [13] \tag{3.4}$$

Which says that accelerated electric charges will be the source for an electromagnetic wave. Here $dP/d\Omega$ is the radiated power to an infinatly small steradian of a large sphere centered around the radiating particle. ϵ is the electric permittivity of the medium the electron is situated in, e is the electric charge, $\hat{\mathbf{r}}$ is the unit vector in radial direction, $\mathbf{u} = c\hat{\mathbf{r}} - \mathbf{v}$ where c is the speed of light and $\mathbf{v}$ is the velocity of the electron and $\mathbf{a}$ is the acceleration of the electron. If one assumes that the incoming electromagnetic wave has an electric component on the form as seen in Equation 3.3, then, according to Newton's second law, the acceleration and velocity will be

Here, electrons located at x=0 are considered?

given by:

$$\mathbf{a} = \frac{eE_0}{m_e}\sin(\omega t)\hat{\mathrm{z}} \tag{3.5}$$

$$\mathbf{v} = \frac{eE_0}{m_e\omega}\cos(\omega t + \alpha)\hat{\mathrm{z}}, \tag{3.6}$$

Here it is looked at electrons located at $x = 0$. α is a constant depending on the initial condition and m_e is the electron mass. By including this in Equation 3.4 one gets that the radiated power per steradian is:

$$\frac{dP}{d\Omega} = \frac{e^4 {E_0}^2}{16\pi^2\epsilon m_e^2 c^3}\frac{\sin^2\omega t_r \sin^2\theta}{(1 - \frac{eE_0}{m_e\omega c}\cos\theta\cos(\omega t_r + \alpha))^5} \tag{3.7}$$

$t_r = t - r/c$ is the retarded time, accounting for the fact that the signal need a finite time to travel the distance r. θ is the angle with the z-axis. A single electron will thus give out electro-magnetic radiation when accelerated by to an electromagnetic wave. However, when one is considering x-ray scattering one is usually not looking at scattering from a single electron, but from the sum of all electrons illuminated by the x-ray beam since electromagnetic waves interact in either a destructive or constructive way, depending on the phases of to wave. To understand this, one first has to look at the scattering from a single atom. The scattering intensity is proportional with the absolute square of the atomic form factor, where the atomic form factor, f^0 is given by:

$$f^0 = \int \rho(\mathbf{r})\mathrm{e}^{i\mathbf{q}\cdot\mathbf{r}}d\mathbf{r}.[14] \tag{3.8}$$

where $\rho(\mathbf{r})$ is the charge density at position $\mathbf{r}$ and $\mathbf{q}$ is given by:

$$\mathbf{q} = \mathbf{k} - \mathbf{k}' \tag{3.9}$$

Where $\mathbf{k}$ and $\mathbf{k}'$ is the incoming and outgoing wave vector. When one is considering the scattering from multiple atoms, one has to make a sum over all atoms with the additional factor $\mathrm{e}^{i\mathbf{q}\cdot\mathbf{r}}$[15] to account for the fact that different atoms will spread with a different phase. As the intensity from the scattering from a single atom is proportional with the atomic form factor, is the intensity from the scattering from multiple atoms proportional with the absolute square of the form factor, F, given by:

$$F(\mathbf{q}) = \sum_j f_j(\mathbf{q})\mathrm{e}^{i\mathbf{q}\cdot\mathbf{r}_j}[14]. \tag{3.10}$$

Here the sum goes over all the different atoms involved, and $f_j(\mathbf{Q})$ is the atomic form factor of atom number j. If the atoms are situated at a lattice with lattice vector $\mathbf{R}$, then the form factor can be described as:

$$F(\mathbf{q}) = \sum_{\tilde{j}} f_{\tilde{j}}(\mathbf{Q})\mathrm{e}^{i\mathbf{q}\cdot\mathbf{r}_{\tilde{j}}}\sum_n \mathrm{e}^{i\mathbf{q}\cdot\mathbf{R}_n}. \tag{3.11}$$

Here $\tilde{j}$ represent the positions of the atoms relative to the lattice point defined by $\mathbf{R}_n$,:

$$\mathbf{R}_n = n_1\mathbf{a}_1 + n_2\mathbf{a}_2 + n_3\mathbf{a}_3. \tag{3.12}$$

$(\mathbf{a}_1, \mathbf{a}_2, \mathbf{a}_3)$ are the basis vectors of the lattice and (n_1, n_2, n_3) are integers. Since n is a large number and all the phase factors $e^{i\mathbf{q}\cdot\mathbf{R}_n}$ will lie on the unit circle, the sum

$$\sum_n e^{i\mathbf{q}\cdot\mathbf{R}_n} \tag{3.13}$$

will go to 0 if

$$\mathbf{q}\cdot\mathbf{R}_n \neq 2\pi m \tag{3.14}$$

where m is an integer. This means that it is only scattering vectors, $\mathbf{q}$, equal to the reciprocal lattice vector, $\mathbf{G}$, that will interfere constructively, since the reciprocal lattice vector has the property

$$\mathbf{G}\cdot\mathbf{R}_n = 2\pi m \tag{3.15}$$

The condition

$$\mathbf{G} = \mathbf{q} \tag{3.16}$$

is called Laues condition, and is also compliant with Braggs law, stating

$$m\lambda = 2d\sin\theta. \tag{3.17}$$

Where m is an integer, λ is the wavelength of the incoming x-ray beam, d is the distance between the same type of planes in a crystal and θ is half the scattering angle 2θ.

3.2.2 Scattering from a non-ideal crystal

The Laue conditions can be described by looking at the Ewald sphere in k-space, as shown in Figure 3.1 (a). Here, all points describe a reciprocal lattice point, and those points that are situated at the sphere that are created by the incoming wave vector $\mathbf{k}$, will fulfill Laues condition. For a perfect crystal, only a few will fulfill the condition, depending on the orientation of the crystal with respect to the incoming beam. If one however have a material without perfect crystallinity, one can look at the situation as taking multiple crystals oriented in different directions to each other in real space, and put all the reciprocal lattices on top of each other i k-space. This is demonstrated in Figure 3.1 (b). Here, one can see that the lattice points have been smeared out, and thus letting more points fulfill Laues condition. This is seen in all three dimensions, thus smearing out the single point over an area in reciprocal space. This means that the scattered beam will not be focused in one single point, but will be smeared out in lobes on the detector. In the extreme case where the material being radiated is a powder, the reciprocal points will be a perfect sphere around the origin in reciprocal space and the diffraction signal will be a circle around the incoming beam.

Since polypropylene consist of a very long chain of molecules it would be believed that one direction would be preferred over the other directions. The molecules will however likely be somewhat tilted with respect to each other and thus not creating a perfect crystal. When then doing a scattering experiment one could expect to not see perfect spots, but lobes centered around the incoming beam.

3.3 Theoretical background for the parameter used in the analysis

There were a number of different parameters analyzed from the diffraction pattern registered by the detector. Figure 5.1 and 3.2 shows an ordinary diffraction pattern and how it was analyzed by the computer program created by Håvard Granlund [1]. The analysis was done by selecting a q-range of interest on the detector image and then fitting it to a Gaussian curve on the form

$$G = A \cdot \mathrm{e}^{\left(\frac{(\theta-\chi)^2}{2d^2}+\frac{(\theta-\chi-180)^2}{2d^2}+\frac{(\theta-\chi+180)^2}{2d^2}\right)}, \tag{3.18}$$

after subtracting the background. Here θ is the angle of the peak of the signal, χ is the angle on the detector image, A is the amplitude and d is the full width at half maximum (FWHM). From this fit one can draw out a number of parameters. The orientation of the scattering signal lies in the parameter θ and can be used for analyzing the preferred direction of the scattering signal.

The visibility was in this project defined as

$$V = \frac{A}{A+B}, \tag{3.19}$$

where A is the amplitude of the gaussian fit, as before, and B is the background, as marked in Figur 3.2. The visibility can say something about the degree of orientation, where a high visibility and a sharp peak would usually mean high order of orientation. Although a high visibility in itself is not a measurement of degree of orientation because the visibility can still be high in an material if the width of the peak is very large. A large width will often come from the fact that the molecules are tilted with respect to each other, as described in section 3.2.2. This can for example happen for a material with strong scattering, but with a certain forbidden orientation. The scattering amplitude can then be generally large, except in a single region where it will be no scattering at all, thus making the visibility large although the degree of orientation is low. The peak width of the scattering signal did however not look alarmingly large in the measurements done in our experiment, and it can therefor be safe to say that a high visibility at least indicates a higher degree of orientation than a low visibility.

The SAXS data was analyzed by a program created by Oliver Bunk [2]. The detector image was sectioned in 16 sections, as shown in Figure 3.3. The q-area of each sections was integrated up to see in which direction each the scattering signal was strongest, for the different q-values. The program also analyzed a number of other parameters based on the fourier components of the signal, but this will not be done in any more detail in this report, and is therefor omitted.

[1] Institute of physics, NTNU
[2] Paul Scherrer Institute

Rart å introdusere dette i en bildetekst?

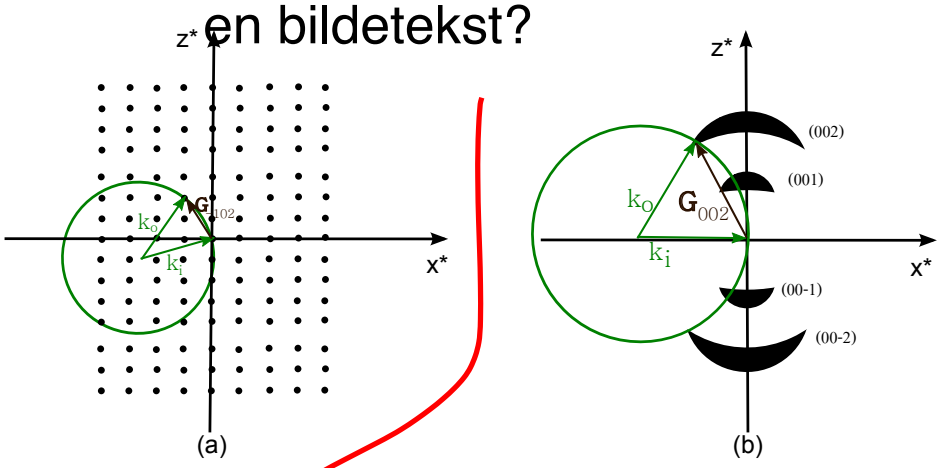

Gå det an å ha det slik med bildetekst

Figure 3.1: a) A cross section of a perfect crystal in reciprocal space. Each point represents a set of scattering planes. $\mathbf{k_i}$ is the incoming wave vector ending at the origin. The Ewald sphere is a sphere with the incoming wave vector as radius. Any reciprocal lattice point intersecting the Ewald sphere will fulfill the scattering criterion and an outgoing wave vector $\mathbf{k_o}$ will follow the path as indicated. $\mathbf{G_{-102}}$ is the reciprocal lattice vector that is equal to the scattering vector $\mathbf{q}$ in this particular case. b) Reciprocal space of a non-perfect crystal. The crystals are rotated with respect to each other along an axis normal to the ones shown. This will spread out the single points (001), (00-1), (002) and (00-2) over an area in reciprocal space. The scattering condition can therefore be fulfilled for different incoming wave vectors, and the outgoing scattering vector can have multiple directions, not just forming a single spot, but lobes, or in a powder; rings.

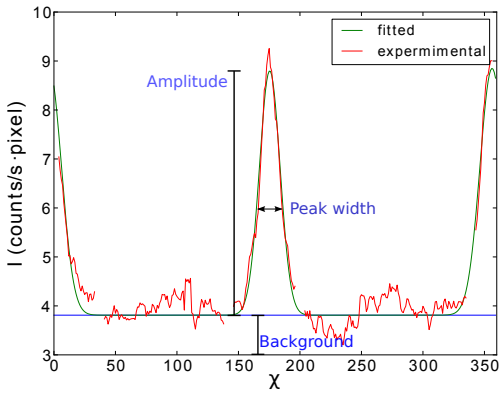

Figure 3.2: A typical signal from the detector. The angle χ is the angle of around the detector image counter clockwise. The red line is the experimental data, while the green is the fitted curve. The background, amplitude and peak width (FWHM) are indicated on the figure.

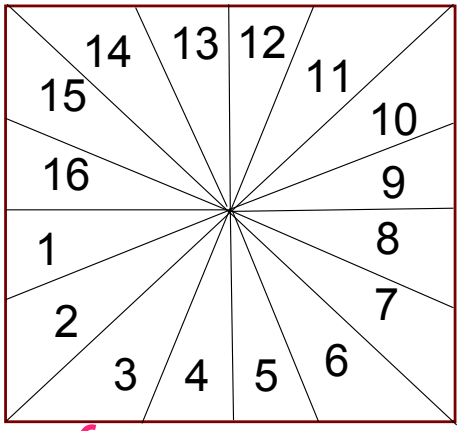

Figure 3.3: In the SAXS analyzis the detector image was sectioned in 16 sections, marked 1-16. The different pixel values for the each q-values in each section was integrated to get at the direction the scattering signal was strongest.

Chapter 4

Experimental

The experimental set up is shown in Figure 4.1. It was used a molybdenum source, which has characteristic x-ray lines at wavelengths 0.7 Å. The width of the x-ray beam was measured to be around 0.2 mm. This was achieved with a series of slits placed before the sample holder. The sample holder was placed on piezoelectric actuators [DETTE MÅ SJEKKES!] which made it possible to move the sample with below mm precision. After the sample holder, a Dectris 1M Pilatus detector was placed, which recorded the scattering signal by counting each photon which hit the detector and storing it in a matrix, depending on which pixel on the detector the photon hit. The experiments were performed by exposing the sample for the x-ray beam for a time between 60 and 200 seconds, depending on which sample was being measured, and at the same time measuring the scattering with the detector. After each exposure time, the sample was moved in either x or y direction and a new recording of the scattering was started. In this way the hole, or parts, of the sample was scanned. The entire experiment was automated, and controlled from a computer.

It was two different kind of samples. One in the shape of a "dog-bone", and one in the shape of the front view of a house. They will further be be referred to as "dog-bone" and "house". The samples can be seen in Figure 4.2. All the different scans done one the samples are shown in Figure 4.3. With an indicated scan number, to make it easier to separate them.

(a) (b)

Figure 4.1: The experimental set up for the experiment. a) Graphical view of the set up. i: Molybdenum x-ray source, ii: x-ray focusing optics, iii: vertical slits, iv: horizontal slits, v: sample, vi: beam stop, vii: detector. b) Real image of the experimental set up.

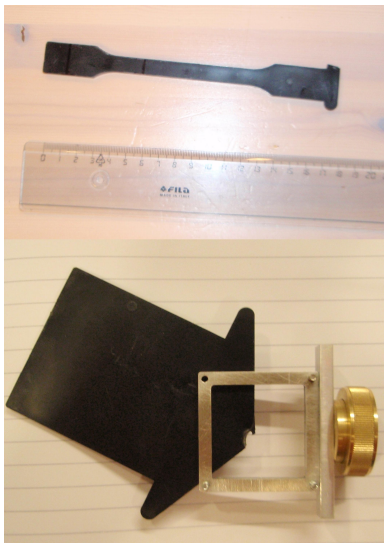

Figure 4.2: The two different samples being measured. The top is the one shaped as a "dog-bone" and the bottom is the one shaped as the front view of a house. At the top of the house ~~one can see the~~ break off edge, where the sample has been broken off from the rest injection mold.

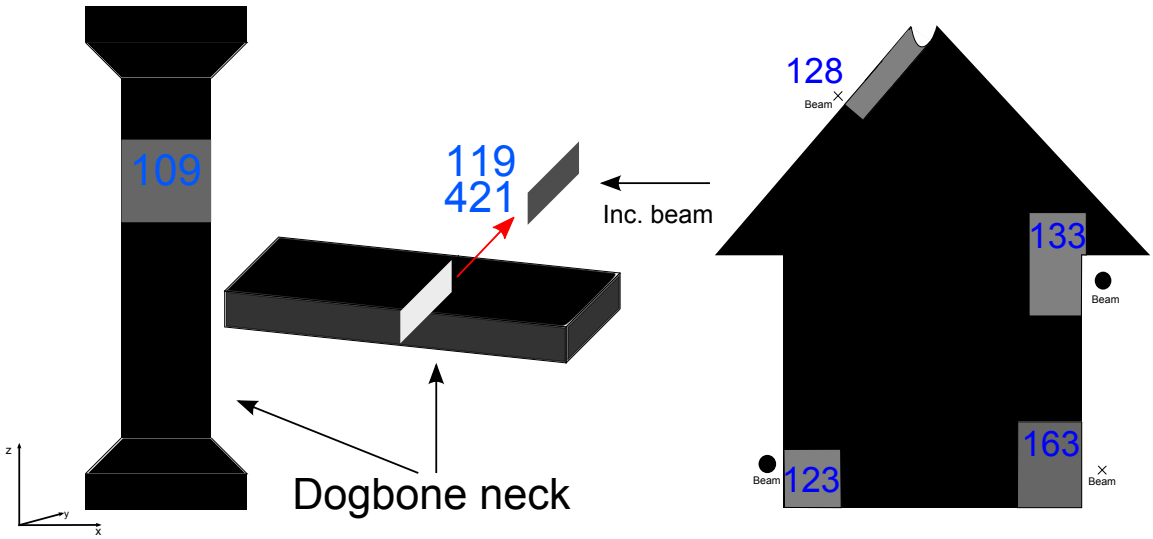

(a) (b)

Figure 4.3: The different scans done on the two samples. (a) Shows the scans done one the dog-bone, with the corresponding scan number, with the x-ray beam in to the page for scan 109. (b) shows the scan done on the house, with the corresponding scan number. The circle beam sign symbolizes that the x-ray beam went out of the page, while the cross beam sign symbolizes that the beam went in to the page. The scan numbers will be used later in the report to separate the different areas that were scanned.

Chapter 5

Results

A typical image from a single diffraction experiment recorded by the detector is shown in Figure 5.1. One notices different kind of rings on the image, which comes from different satisfactions of the scattering criterion as discussed in section 3.2. The scattering signal is however not isotropic but is concentrated around a peak value.

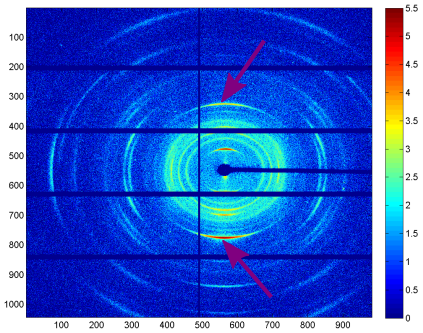

Figure 5.1: A typical diffraction image from the polypropylene samples. The colorbar to the right indicates the number of counts on a logarithmic scale. One can see a number of different diffraction circles, which has the intensities focused at specific areas of the circle. This indicates that it is some kind of preferred direction, and not a random orientation. The rest of this analysis has been focused on the ring marked with the purple arrows. The dark blue lines comes from the fact that the detector consist of different modules, and also the beam stop.

The large number of rings could make it possible with a deep analysis of the the images, where the different rings where analyzed separately. It was however noted that, to eye measurement, the alignment of many of the different rings all followed the same pattern in such a way that when the bright diffraction pattern marked with the purple arrows in Figure 5.1 rotated, the rest of the rings rotated an equal amount in the same direction. The development of the direction of the scattering signal would therefore be very similar between the rings. Although the visibility would be different for the different diffraction patterns, it was decided to only make an analysis of the development of the ring marked with the purple arrows. This ring is the $(hkl) = (006)$ reflection of talc [1].

Jeg skjønner ikke så mye av siste avsnittet her

5.1 Scan of dog-bone neck

The results from the scan of the dog-bone neck in the xz-plane, marked with scan number 109 in Figure 4.3 (a), are given in Figure 5.2 and 5.3.

The orientation of the scattering signal is clearly aligning itself perpendicular to the edge of the sample, and the orientation is strongest closer to the edge, as indicated by the brightness of the color. The orientation is also in general stronger at the right part of the sample compared to the left. Closer to the center the orientation breaks down, as indicated by the black color, which indicates that there is no preferred orientation.

When comparing the two different plots, one can notice that the plotting parameter is not symmetric around the center of the sample, but shifted to the right. One can also see that the orientation and visibility are clearly stronger in the right part of the sample. Both the parameters are also strongly affected by the edge of the sample. This is especially visible in Figure 5.3 where the parameter value is highest towards the edge. From the visibility plot, one can notice that the plotting parameter stays high (the red area) for roughly the same distance inwards in the sample, for both sides, but the visibility in the right part drops down much quicker to a lower value compared to the left part.

5.2 High resolution scan of dog-bone neck cross section

The plots for scan 119, where the incoming x-ray beam was incident at the cross section of the dog-bone neck, as illustrated in Figure 4.3, are given in Figure 5.4 and 5.5. This scan was done with high resolution, to see higher details among the different part of the sample.

Figure 5.4 shows the orientation of the diffraction pattern in the sample. It is clearly strongly affected by the edges of the sample, as indicated by the bright colors. The orientation goes from a gradual alignment perpendicular to the left edge to be oriented perpendicular to the top, or bottom, edge. The orientation is symmetric along the horizontal center line with no special feature standing out compared to the rest of the sample.

The visibility shown in Figure 5.5 is high throughout the sample, and only dropping at the center to the right of the sample. The visibility is large in the middle of the sample, and falling a little above and below, which forms an area stretching out to the corners. This feature can not be observed in Figure 5.4, and this indicates that the reason for this formation might not be directly caused by the orientation of the molecules. The edges at the top and bottom seems to have a lower visibility than what it is a small distance towards the center of the sample. This is different than what one observes in Figure 5.3, where the visibility where strongest at the edges. The top and bottom edges are however not the same edges as the top and bottom

edge in scan 109. Here, the top edge would be the same as the front side of scan 109. The right edge of scan 119 is the left edge seen in scan 109. At this edge in scan 119 the visibility is also highest as it is in Figure 5.3.

5.3 Low resolution scan of dog-bone neck cross section

A low resolution scan over the entire cross section of the dog-bone neck, marked as scan number 421, is shown in Figure 5.6 and 5.7. All of these plots have a white marking at the top right corner, ~~and this~~ which is caused by the sample holder, and not the sample itself.

The orientation of the scattering signal, shown in Figure 5.6, is clearly affected by the edges. The orientation of the scattering is gradually turning from being perpendicular to the top and bottom edges, to be perpendicular to the left and right edges, as seen in Figure 5.4. One can see that the orientation is roughly symmetric around a horizontal line through the sample center, but it is not symmetric around a vertical line through the center. Here, it is shifted to the left of the sample, and this is in agreement with the decentering seen in Figure 5.2 and 5.3. The reason why the decentering in the cross section is to the left, and in the dog-bone neck to the right, is because the incident beam was in the positive y-direction for the dog-bone neck scan, while it was in the negative z-direction for cross section scan. The decentering is therefore located at the same place in the sample, and not caused by other effects.

In Figure 5.7, ~~one can see~~ the same kind of development where a horizontal V-shape stretches out from the center towards the corners in both directions. An interesting observable is that the value of the visibility is not the same on both sides. In Figure 5.7 one can see that the visibility is higher to the left part, compared to the right part. One can clearly see that the visibility is higher in the bottom part of the sample, compared to the upper part, and the left part also has a higher visibility compared to the right part.

5.4 Scan of left and right corner of house sample

The results for the scans around the two bottom corners of the house, marked as scan number 123 and 163, are presented in Figure 5.8 and 5.10. The scan of the right corner is of a larger length scale, but with the same resolution.

The orientation plotted in Figure 5.8 is done with a different method than the rest. This was done to emphasize bending from the vertical edges towards the corner, and the discontinuity in direction above the bottom edge, where the changing of the orientation is much larger than the resolution of the scan. This was also observed by looking at the image data from the detector. The choice of this kind of plot is also based on the factor that this gives somewhat better information on the strength of the orientation in this case, where the length of the bar symbolizes how strongly

Det hadde vært veldig fint å ikke ha alle bildene samlet på slutten, men heller spredd litt rundt

that area is oriented. One can see that the orientation is strong along the edges, but decreases significantly when one moves inwards in the sample. Close to the bottom one can observe that the development of the direction seem to have a discontinuity in the horizontal component of the orientation gradient. The orientation of the scattering signal suddenly jumps to a different value. This effect is shown in Figure 5.9. It doesn't seem to be any major differences between the to corner areas of the sample with regard to the orientation.

The visibility of the two corner areas, as shown in Figure 5.10, also looks to be fairly similar, as it did for the orientation. The visibility is clearly strongest at the edges, and decreasing inwards in the sample. An interesting part is at the corner, where a region of low visibility is sliding under a part of high visibility near the bottom. This can be seen for both corners, but the effect looks to be strongest for the left corner.

5.5 Scan of area between wall and roof of house

The orientation and visibility of the section of the house around the area of the house wall and house roof, as indicated by scan number 133 in Figure 4.3 is shown in Figure 5.11. They all show much of the same tendencies, where the plotting parameter is highest towards the edge, and decreasing inwards. One can note an effect at about 8.5 mm and 13 mm, where one can see a clear line in both plots. This is an area where the sample thickness was reduced, and the thin part was in the area [8.5 mm,13 mm]. In Figure 5.11 (b) one can see that the visibility falls down quicker in the area of low thickness, but the maximum value looks to be the same as the maximum value in the area with thick thickness.

5.6 Scan around breaking area of house

The results of the analyzes of scan 128, which was over the top of the roof of the house, are given in Figure 5.12 and 5.13. One can in Figure 5.12 see that the orientation of the scattering sample is rotating as one follows the breaking point, which is at the lower part of the scan. the scattering signal is therefor not aligning itself either perpendicular or parallel to the edge of the breaking point, but rather both, depending on where along the edge one looks. Along the vertical edge the orientation is slightly tilted compared to the edge, and not aligning itself perpendicular to the edge surface until a little distance inside the sample. This has not been observed in the previous scans, where the alignment has always been perpendicular to the edge. The strength of the orientation can also look to be slightly lower at the edge, than a small distance inside.

The visibility shown in Figure 5.13 show that some parts around the breaking point forms regions with high visibility, while other regions have low visibility. At the vertical edge one can see that the visibility is not strongest along the very edge, but is increasing a small distance inwards. The area with high visibility seems to

coincide with the part at the orientation plot that has a bright blue region, a small distance from the vertical edge.

5.7 Small angle x-ray scattering

A typical diffraction signal from the ED-samples is shown in Figure 5.14. Figure 5.14 (a) shows the direction of the scattering pattern, while Figure 5.14 (b) shows how the signal varies as function of q for 16-different sections of the detector. One can see that there are many different diffraction peaks in the signal. For the further analysis the q-area of $q = 0.002$-0.007 Å^{-1} was used, as marked in Figure 5.14 (b).

The orientation of the scattering signal for low q for small angle X-ray scattering is given in Figure 5.15. It is highly visible that the scattering signal also for SAXS measurements are oriented perpendicular to the edge, in the same way as for WAXS. Since the measurements are done on different kind of samples, with different shear rates, and different temperatures, one can notice differences in the plot. Those samples manufactured with high shear rate have a feature to the right of the sample, which is marked with a black ring in Figure 5.15 (i). Here it is visible that the dark and bright blue area turns upwards. This is visible for all samples with high shear rate, but only on one of the sides. This feature is not visible for low or medium shear rate, and one can not find it in Figure 5.15 (a) as one should expect if this feature would happen for lower shear rates. The black line in Figure 5.15 (d) shows the area where a 1 dimensional line scan of the orientation were done. This was done to see more of the development of what happened in the region the black rings are marking.

Figure 5.16 shows the orientation of the scattering signal through a single vertical line of the samples EDLL, EDLH, EDML, EDMH, EDHL and EDHH. One can see that it looks like the absolute value of the orientation is higher in the samples with low shear rate compared the samples with high shear rate, for the same temperature. When the temperature is rising, the difference in orientation seems to vanish.

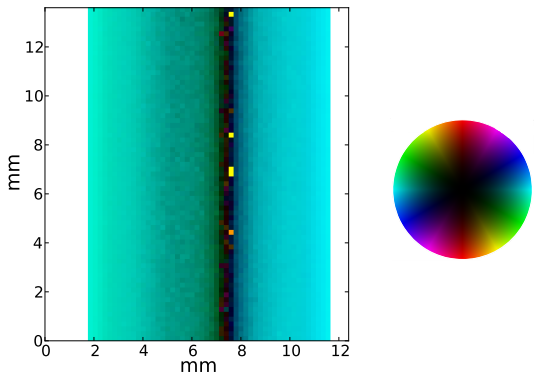

Figure 5.2: The orientation of the scattering pattern from scan 109. One can clearly see that the diffraction pattern align itself with the edges of the dog-bone. The color of the plot is giving the direction of the scattering pattern as indicated by the color wheel, while the gray scale is symbolizing how aligned it is. Towards the center one can notice that the color turns black, which means that it is no preferred alignment. This does however not happen at the symmetric center of the dog-bone neck, which one could assume, if everything in the production face was symmetric.

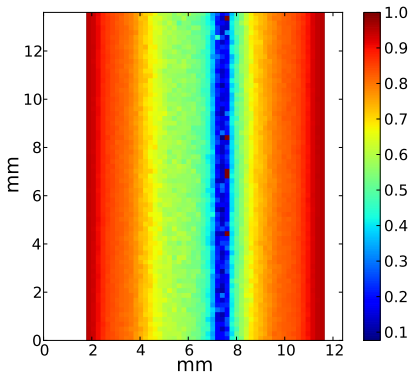

Figure 5.3: The visibility from scan 109 of the diffraction pattern is highest at the edges of the sample, and slowly decreasing towards the center. This is consistent with Figure 5.2 where it was no preferred orientation at the center, which was located to the right of the symmetric center of the dog-bone. One can see some dark red pixels at the center, which is most likely caused by a failure in the analyzing routing, because of the lack of preferred scattering direction.

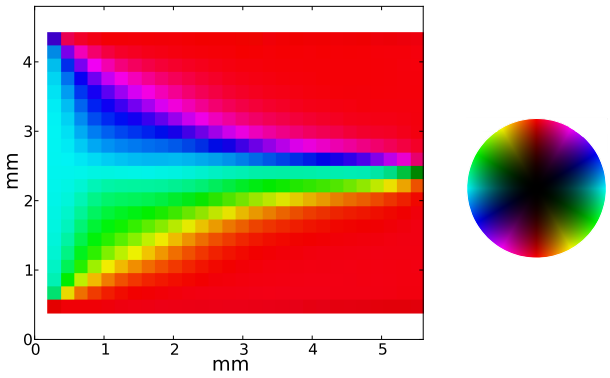

Figure 5.4: The orientation of the scattering signal from scan 119. The orientation plot of the cross section of the dog-bone neck. One can clearly see a strong alignment toward the edges of the sample, as indicated by the red color and light blue color. It is also a gradual transition between the vertical edge and the horizontal edges.

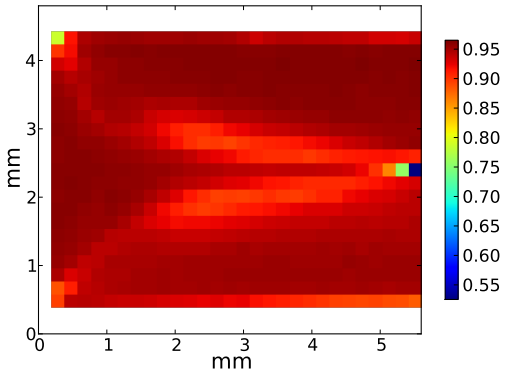

Figure 5.5: The visibility from scan 119. The visibility of the cross section of the dog-bone neck. It is a high visibility throughout the sample. The only exception is at the very center, where the visibility drops to 0.55. Since the visibility is high, the amplitude of the scattering signal is high compared to the background. This can indicate a high degree of orientation, because the scattered signal is probably not spread out over a ring, but concentrated at the peaks. One can also see that it seems like the visibility is higher in the top part of the sample, compared to the bottom part.

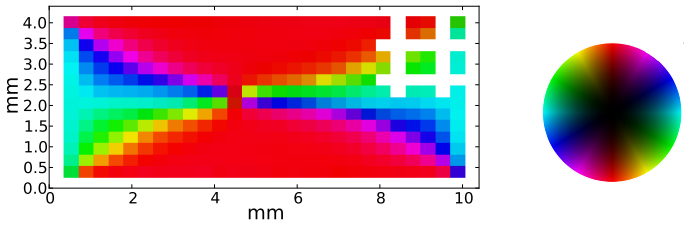

Figure 5.6: Scan 421: The orientation of the scattered signal is aligning itself perpendicular to the edges. This is similar to both Figure 5.2 and Figure 5.4. One can also see that the development of the alignment of the scattered signal is not symmetric to the sample geometry. This is consistent with Figure 5.2 and 5.3 where it was observed that the signal symmetry was shifted to the right. Here the symmetry is however shifted to the left, but this is because the incoming x-ray beam was oriented in the negative z-direction, while in scan 109 the beam was oriented in the positive y-direction. See Figure 4.3 (a) for explanation of the coordinates. The white mark in the top right corner is due to the sample holder.

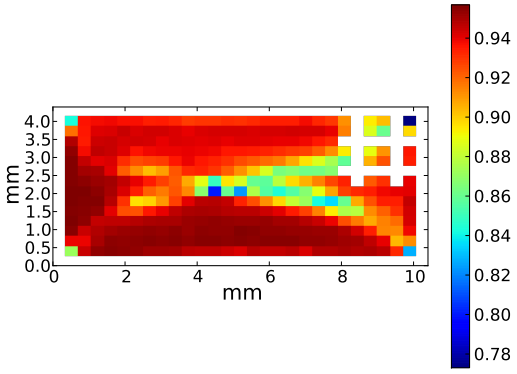

Figure 5.7: Scan 421: The visibility of the scattering signal is high throughout the sample. The left part of the sample has a clearly higher visibility than the right part. When comparing to the high resolution scan in Figure 5.5 one can see that they are clearly consistent with each other, but the shapes are much harder to recognize in the low resolution plot, as expected. The visibility symmetry is also clearly shifted to the left of the center, as was the case for the orientation.

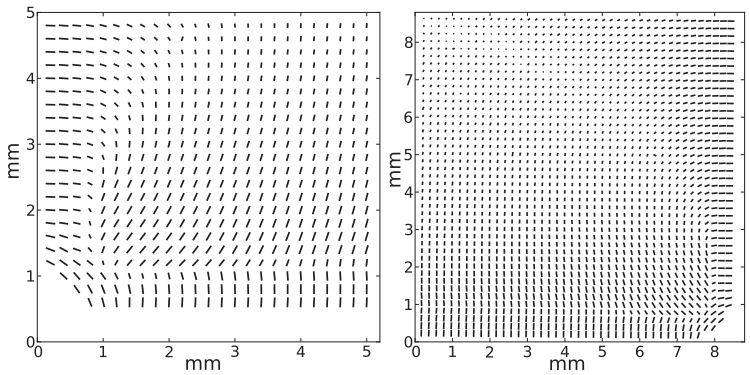

(a) (b)

Figure 5.8: The direction of the scattering signal of from the two bottom corner of the house. a) scan 123, b) scan 163. It is a rather strong orientation in both corner of the house, where the length of the lines symbolizes how strong the orientation is. One can clearly see that the orientation is directed towards the corner of the sample. At the edges the scattering signal is orienting itself perpendicular with the surface, except at the corner, where the scattering signal is aligning itself parallel to the edge. Close to the bottom a discontinuity of the horizontal component of the directional gradient is visible.

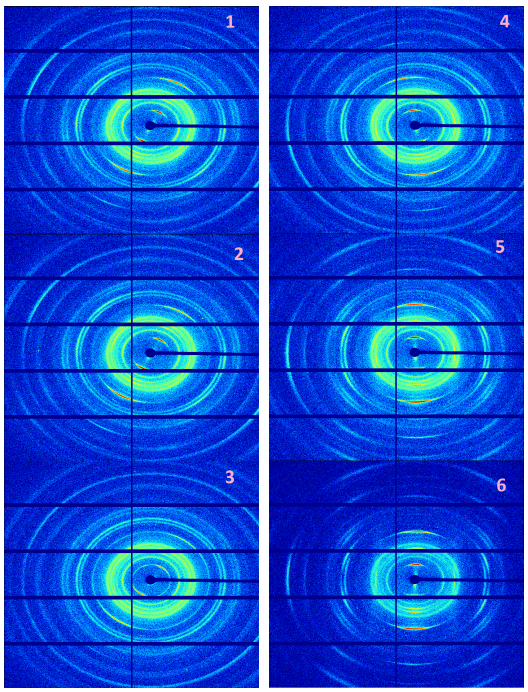

Figure 5.9: The detector images shows a column of images from scan 123 near the bottom of the sample. One can clearly see a sudden discontinuity between image 3 and 4 by looking at the innermost diffraction pattern.

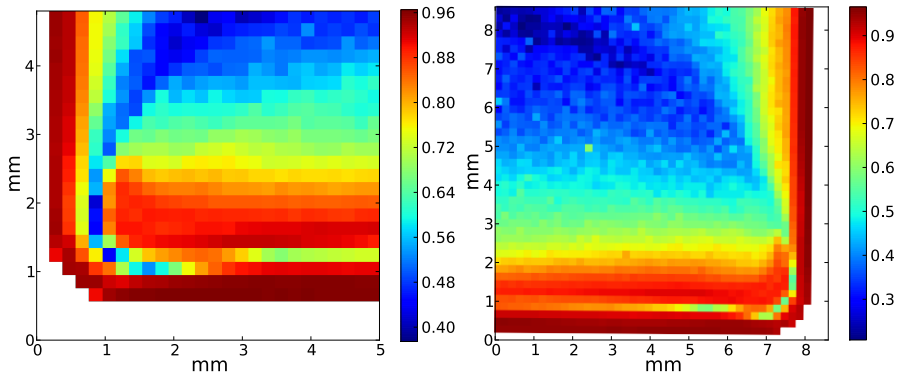

(a) (b)

Figure 5.10: The visibility of the two bottom corners is strongest toward the edges, and decreasing towards the center of the sample. It can be noticed that it is a small area of low visibility sliding between two areas with high visibility near the bottom. The sample looks to be symmetric from just looking at the corners. In the horizontal direction the visibility is highest at the edge, as seen in previous scans.

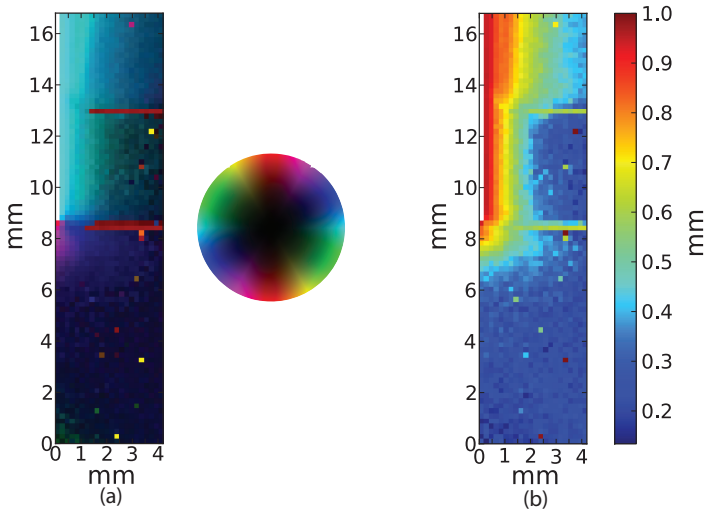

Figure 5.11: Scan 133: a) The orientation of the diffraction pattern is strongly oriented perpendicular to the surface edge. It is however quickly becoming weaker as one moves inwards the sample, as indicated by the fact that the colors become darker. Red horizontal lines at 8.5 mm and 13 mm in vertical direction is caused by the fact that this area was a transition between a high to a slightly lower thickness of the sample. b) The visibility is clearly highest toward the edge. One can note that the visibility drops off quicker in the thin part of the sample, between 8.5 mm - 13 mm in vertical direction, which is most likely caused by the fact that it is less scattering material and therefor the background will be relatively larger.

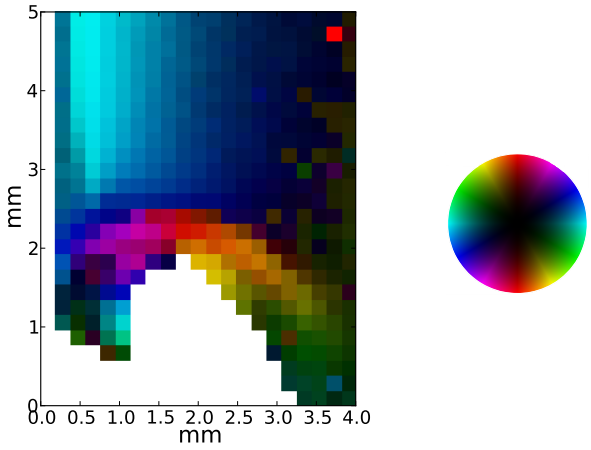

Figure 5.12: Scan 128: The orientation of the scattering signal shows that the alignment at the edge is slightly weaker compared to a small distance inside the sample, and also tilted compared to the surface. At the point where the sample has be broken loose from the mold, forming a reversed U at the bottom, the alignment is starting at the right part on the green part of the scale, and turning clockwise as one follows the edge at the break of point. It is thus no specific alignment with the edge, but breaking of the polypropylene chains does clearly not form stochastic variations in the direction.

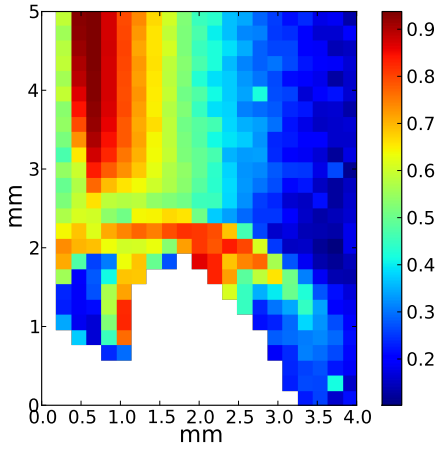

Figure 5.13: Scan 128: The visibility is highest a small distance from the vertical edge, which match the pattern seen in Figure 5.12. Along the breaking point, the visibility varies between 0.3 and 0.8. This indicates that how the breaking occurs can have significant effects on the macroscopic scale. At the end of the peninsula, at the bottom left, the visibility is less than to the right and above.

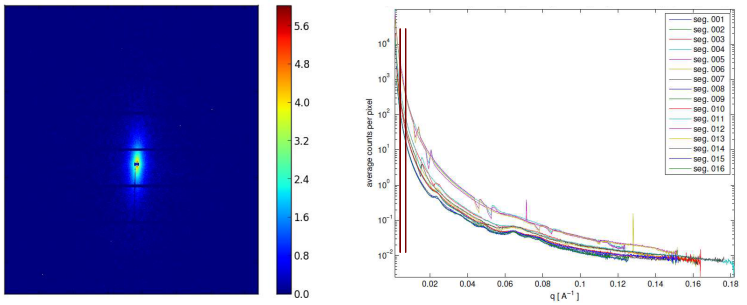

(a) (b)

Figure 5.14: a) A typical diffraction image of the small angle x-ray scattering experiment. It is clearly a direction of the diffraction pattern centered around the beam stop. b) The detector image has been sectioned in 16 sections and the diffraction pattern has been integrated up for each q-value. The area between the two red bars represents the q-area which was analyzed.

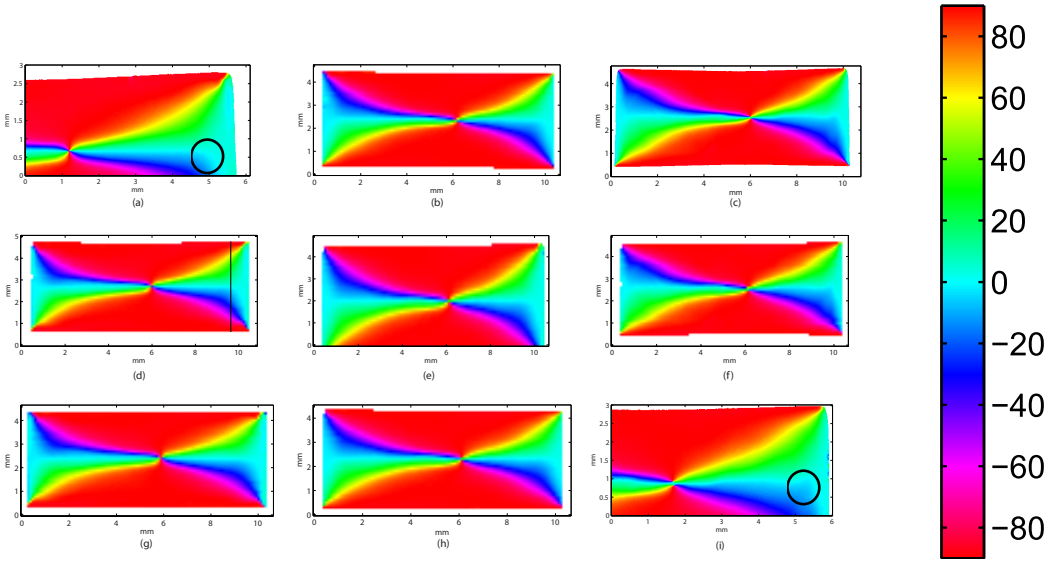

Figure 5.15: Development of orientation as function of shear rate and temperatur for low q. Shear rate is increasing from left to right, temperature is increasing from top to bottom a) EDLL, b) EDLM, c) EDLH, d) EDML, e) EDMM, f) EDMH, g) EDHL, h) EDHM, i) EDHH. The colorbar symbolizes the orientation of the diffraction peaks in degrees. The orientation of the diffraction pattern is clearly aligning itself perpendicular with the edges of the sample. Inside the black ring in figure (i) one can see a feature, where the dark blue orientation is turning slightly up, this is visible only for high shear rates, and only for one of the sides of the sample. One can not see this feature inside the black ring in figure (a), as one should expect, if this occurred for lower shear rates. The black line in figure (d) is indicating where the data for the 1D line plots in Figure 5.16 are taken from.

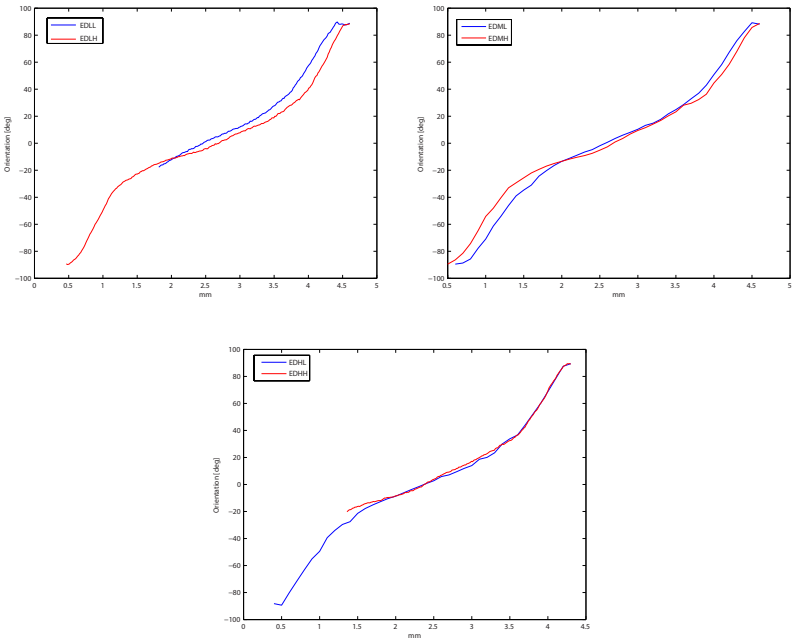

Figure 5.16: 1 dimensional orientation plots of the SAXS data. (a) EDLL and EDLH, (b) EDML and EDMH, (c) EDHL and EDHH. The data is taken from roughly the same region on all the different samples. It can look like the orientation is more aligned towards the top and bottom edge of the samples, as seen in figure (a) and (b), but that a higher temperature is equalizing this effect, as seen by the development of the differences between the curves, from (a) to (c).

Chapter 6

Discussion

6.1 Edge effects on the scattering orientation

One can clearly see from the figures in Chapter 5 that the scattering signal is strongly affected by the edges of the sample. The orientation prefers to align itself perpendicular to the edges, as seen in Figure 5.2, 5.4, 5.6, 5.8, 5.11 (a) and 5.12. From Figure 5.2 and 5.6 one can also see that the orientation is not symmetric around the center of the sample. It can be hypothesized that this is caused by the manufacturing procedure. The dog-bone is manufactured by injecting melted polypropylene at one of the sides. This flow can cause the shift in alignment of the symmetry of the orientation compared to the sample center. This effect can also be caused by the temperature gradient across the sample. During the manufacturing of the samples, one side of the dog-bone will have a slightly higher temperature than the other side. This difference in temperature across the sample can cause different parts of the sample to crystallize at different times. The shifting of this alignment can be believed to cause some mechanical effects, although this has not been tested. To see what kind of mechanical effects this could have, it would be needed to make different samples, under different conditions. Suggestions for testing how the injection and temperature gradients affect the sample could be testing different samples where the polypropylene has been injected to the mold from both sides, and different temperature gradients should be tested.

All the plots of the cross section of the dog-bone show a significant sectioning of the sample, as seen in Figure 5.4 - 5.7. These figures indicates that one can section the sample in to four regions, the top, bottom, left and right part that has the talc c-axis direction towards the edge, as indicated by Figure 6.1. This is consistent with the directional and visibility plots in Figure 5.2 and 5.3 which is of the front view of the dog bone neck. In this scan the scattering vector will only be able to be equal the reciprocal lattice vector when it points to the sides, which is in area III and IV in Figure 6.1, and not towards the front or the back, which is in area I and II. This can be visualized by looking at Figure 3.1 (b). In scan 109 the x-ray beam will see the reciprocal space as indicated in Figure 3.1 (b) in region III and IV, while in region I and II the x-ray beam will see a reciprocal space where the $\mathbf{x}^*$ and $\mathbf{z}^*$ axis is rotated 90°, without moving the incoming x-ray beam. The reciprocal lattice points can then not intersect the Ewald sphere and no scattering will occur. The

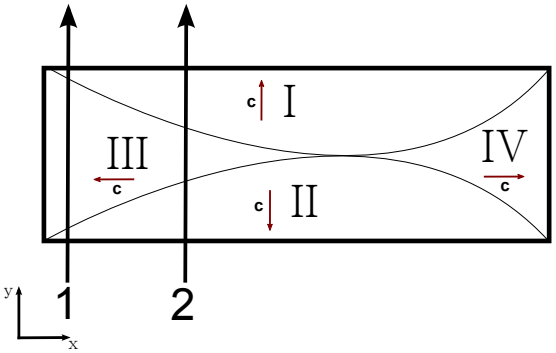

Figure 6.1: The areas of the cross section of the dog bone can be sectioned in to four different areas based on the direction of the scattering pattern. The direction of the scattering pattern is the direction of one of the reciprocal lattice vectors to the sample. The two black lines symbolize the line the x-ray beam is traveling when the dog-bone is being scanned from the front. As one can see, line 1 travels through a large part where the reciprocal lattice vector points to the right, while much of the distance line 2 travels through goes through area I and II, where the c-axis points along the beam, thus making it impossible to fulfill the scattering condition.

visibility becomes lower towards the center because the x-ray beam travels through less material where the scattering condition can be fulfilled. At the very edge, the x-ray beam travels through almost only an area with the reciprocal lattice vector in the right direction, while closer to the center a large part of the path the x-ray beam transverse is through section I and II, thus not contributing to the scattering. This is indicated in Figure 6.1. The visibility, which is an indication of degree of orientation, will therefor seem less towards the center of the sample, because a large part of the orientation of the sample will not have a reciprocal lattice vector which fulfills the scattering conditions compared to the edges. When comparing the orientation in Figure 5.2 and visibility in Figure 5.3 of the dog-bone neck with the orientation in Figure 5.8 and the visibility in Figure 5.10 it makes it plausible that the orientation of the relevant reciprocal lattice vector is the same in the house as the dog-bone. The preferred direction of the c-axis is hence towards the edges, with similar sections of the cross sections as in Figure **??**. When looking close to the center of the house, almost none of the molecules will have a direction that can fulfill the scattering conditions, therefor the visibility will be very low towards the center. This can however not be fully verified without doing a measurement of the cross section of the house sample.

The effect the edges has on the orientation is especially visible Figure 5.11. The transition from high thickness to low thickness at 8.5 mm and 13 mm in the vertical direction shows that any kind of edge will strongly affect the orientation of the crystalline material. In this figure one can also see that the visibility will be high further in in the thick part of the sample compared to the thin part. This makes sense because with more material the more material that can order itself. It is however not just influenced by the amount of material, it can also just be an indication that more material will scatter more. More material means more scattering.

6.2 Effect on mechanical breaking of the sample

In Figure 5.12 and 5.13 the effect of breaking off the polypropylene sample from the injection mold is shown. From Figure 5.12 it can look like one of the molecular c-axis will align itself parallel to the breaking edge, but that some parts along the breaking edge has to have the molecular axes directed perpendicular to the edge. One reason for this alignment could be that the area of where the polypropylene was injected to the mold will have a strong directional alignment in the flow direction. This can be justified by the fact that around the breaking point all the directions looks to flow upwards. This flow seems to affect the direction at the center of the sample, which is tilted slightly upwards to the right. Another reason for this alignment around the breaking point could be caused by the physical breaking itself. When the sample is removed from the injection mold the breaking of the sample will cause the molecular axes to turn and be broken off in such a way as to align itself along the edge. If this is indeed the case, then one can imagine that it can be possible to manipulate the orientation around macroscopic areas by in some ways alter the sample physically.

As seen in Figure 5.13 one can also notice that the visibility is higher around the breaking edge. The breaking edge seems to go quite far in to the sample. It is thus likely that this high visibility is directly caused by the breaking, and not just because the breaking edge is close to where the polypropylene was injected, and the degree of orientation is just a result of the closeness to the injection. In all other measurements, the visibility drops off quite fast towards the center of the sample, and it is unlikely that the visibility would stay as high as it is at the breaking edge 1 mm towards the center from the edge. To see more of what could cause the effect of the alignment along the breaking edge, it would be needed to be made measurements on samples with a cleaner breaking edge, and also with breaking edge that doesn't go as deep as the one in this sample does.

It can be speculated that the talc c-axis is not the reason for the alignment. It could well be one of the axes of polypropylene that align itself, and this drags the c-axis with it. It could be believed that the axis along the long chain of polypropylene will align itself along the cut edge. This could then position the c-axis of talc in such a way that it will some places align itself parallel to the edge, and some places normal to the edge. To further analyze what happens at the edge, it would be needed to see how the axes of polypropylene behaves close to the edge.

6.3 Image artifacts

In many of the pictures one can see some pixels with a completely different value compared to the surroundings. This is for example visible in Figure 5.11 (b) where it is some dark red pixels close to the bottom of the figure. Also Figure 5.2 show some pixels with a bright yellow color, compared to the dark regions around, at roughly 7.5 mm in horizontal direction. This could be caused by the fact that the scattering peaks are very low, making it hard for the plotting routine to fit a correct curve to the data set, since the peaks are low compared to the background, and fluctuations

in the background could be registered as a peak. The bright yellow pixels coincide with the pixels with high visibility at the center of the sample in Figure 5.3. This sudden rise in visibility seems unlikely when one considers the surroundings, and it was not observed any sudden rise in scattering intensity at the center of the sample from the images from the detector. It is therefor likely that the fitting routine failed in these pixels, due to the low scattering peaks.

6.4 Small angle x-ray scattering

Figure 5.15 shows that the general tendency for all the different ED-samples are very similar with each other, where the alignment of the scattering pattern in perpendicular to the edges of the sample. This is also very similar to what was observed for the wide angle x-ray scattering experiment. The samples measured contained a lot of talc that spreads x-rays more than what polypropylene does. It is therefore likely that the scattered signal is more influenced by talc, than for iPP.

The feature which is marked by a black circle in Figure 5.15 (i) indicates that the shear rate has influence on the orientation of the scattering signal. Since one can only see this feature on one of the side for high shear rates, it is plausible that it is partially caused by asymmetry in the injection of the polypropylene to the sample.

The orientations shown in Figure 5.16 shows that the scattering signal is more directed towards the top and bottom edge for lower shear rates, but that an increasing temperature is equalizing this difference. It could be speculated that a higher shear rate makes it harder for the molecules to be ordered toward the top and bottom edge, but that a higher temperature the movement of the molecules makes it possible to align themselves.

Chapter 7

Conclusion

It has been shown that the talc particles in injection molded isotactic polypropylene will align itself with it's c-axis towards the edges of the sample, and that any kind of edge will have strong effect on the alignment, either the edge of the sample itself, or internal edges separating different thicknesses. This effect is verified for a sample shaped as a dog-bone, but it is also likely that this will occur for other shapes, like a house. This analysis covered however only talc, and did not look more at the scattering from polypropylene. Later work based on the same data also covered the alignment of the polypropylene, and it was discovered that the b-axis of polypropylene is aligned in the same direction as the talc c-axis [1]. The article this is described in is attached as appendix A.

Also the scattering signal from the small angle x-ray scattering experiment of the different talc filled iPP samples manufactured under different conditions show strong alignment parallel to the surface normal. It was also discovered that different shear rate and temperature has implications on the orientation. A high shear rate would form a peninsula in orientation compared to the surroundings, but only for one of the sides. The samples manufactured with low shear rate seemed to have a scattering pattern aligned more towards the top and bottom part of the sample, compared to the samples manufactured with high shear rate, but that this difference becomes smaller with increasing temperature. It is not yet clear what direct implications this has on the internal structure, but encourage further studies on the sample since it shows directional alignment, and therefor can ble related to the alignment shown in the WAXS regime.

The production method also seem to influence the symmetry of the orientation of the sample, since this is not symmetric compared to the center of the sample. Effects as a temperature gradient across the mold and the way the melted polypropylene will enter the mold can be reasons for this effect, and a continued study on these effects could give answers to why the misalignment occurs, and what kind of mechanical effects is has on the sample. A thin layer of lower orientation formed in the sample shapes as a house between the lower edge and the interior which coincide with a discontinuity in the vertical gradient of the orientation development. This discontinuity is not yet understood, but a further analysis of the flow of the polypropylene in to the mold could give an explanation to this.

It is also seen that mechanically breaking the sample will have large implications on the orientation of the c-axis to talc. The orientation and visibility is much stronger along the edge. The exact reason for this is unknown, but with further studies one can perhaps find a way of manipulate the direction of the crystalline axis close to the surface by mechanically altering the macroscopic sample.

Bibliography

[1] H. Granlund, J. B. Fløystad, M. Esmaeili, E. T. Bakken, M. Bech, P. E. Vullum, E. Andreassen, and D. W. Breiby, "Mapping structural gradients in isotactic polypropylene using scanning wide-angle x-ray scattering."

[2] C. M. I. Consulting, "Market study: Polypropylene," 2012. Available online.

[3] R. Kongsmo, "Prosjektrapport," Master's thesis, Norwegian University of Science and Technology, 2012.

[4] F. P. van der Burgt, *Crystallization of isotactic polypropylene The influence of stereo-defects*. PhD thesis, Technische Universiteit Eindhoven, 2002. ISBN 90-386-2674-6.

[5] "Wikipedia: polypropylene." http://en.wikipedia.org/wiki/Polypropylene.

[6] M. A. G. C. Marco, G. Ellis and J. M. Arribas, "Analysis of the dynamic crystallisation of isotactic polypropylene/α-nucleating agent systems by dsc," *Thermal Analysis and Calorimetry*, vol. 68, pp. 61–74, 2002. Available online.

[7] S. Z. D. Cheng, J. J. Janimak, and J. Rodriguez, "Crystalline structures of polypropylene homo- and copolymers," *Polypropylene: Structure, blends and composites*, vol. 1, pp. 31–52, 1995. Available online.

[8] F. Khoury, "The spherulitic crystallization of isotactic polypropylene from solution: On the evolution of monoclinic spherulites from dendritic chain-folded crystal precursors1," *JOURNAL OF RESEARCH of the National Bureau of Standards -A Physics and Chemistry*, vol. 70A, no. 1, 1966. Available online.

[9] Y. Wang, C. Chen, J.-Z. Xu, J. Lei, Y. Mao, Z.-M. Li, and B. S. Hsiao, "Suppressing of γ-crystal formation in metallocene-based isotactic polypropylene during isothermal crystallization under shear flow," *The Journal of Physical Chemistry B*, vol. 116, no. 16, pp. 5056–5063, 2012. Available online.

[10] R. H. Todd, D. K. Allen, and L. Alting, *Manufacturing Processes Reference Guide*. Industrial Press Inc, first ed., 1994.

[11] R. A. Phillips and M. D. Wolkowicz, *Polypropylene Handbook*. Hanser, 2005.

[12] B. E. A. Saleh and M. C. Teich, *Fundamentals of photonics*. Wiley, second ed., 2007.

[13] D. J. Griffiths, *Introduction to electrodynamics*. Pearson, third ed., 2008.

[14] J. Als-Nilsen and D. McMorrow, *Elements of modern x-ray physics*. Wiley, second ed., 2010.

[15] C. Kittel, *Introduction to Solid State Physics*. Wiley, eighth ed., 2005.